Proceedings of the 21st ICSMGE, Vienna, Austria, 14 – 19 June 2026. Pistrol, Adam & Schweiger (eds.)
Published by: ÖGG, Austrian Society for Geomechanics, Salzburg, Austria, ISBN 978-3-9503898-4-5
https://doi.org/10.53243/ICSMGE2026-982

AI-Based Parametric Study: Learning from the Past for Resilient Designs

Ye Win (Douglas) Tun, Natalie Murphy, Nidula Jayawardana
Geotechnical and Tunnels, WSP, Brisbane, Australia, douglas.tun@wsp.com

ABSTRACT: This paper presents a parametric study of the coefficient of secondary compression parameters 'C_a' ($(1 + e_0)\, C_{\alpha\varepsilon}$) by back analysis of 40 years of monitoring data using Plaxis2D Finite Element (FE) models and S1MBA (Settlement 1-Dimensional Monitoring Back Analysis). The Soft Soil Creep (SSC) constitutive model (Hypothesis B) is used in Plaxis2D. Although the main objective is to analyse the C_a, other primary consolidation design parameters must be incorporated into the SSC due to its critical assumption that secondary compression (creep) occurs in tandem with primary consolidation. The proposed methodology, which incorporates a fitness function 'F_{PGA}', is a concept that demonstrates the design accuracy and workflow for using monitoring data from different locations in combination with S1MBA. This parametric study aims to enhance design accuracy. S1MBA is WSP's in-house Artificial Intelligence (AI)-based genetic algorithm (GA) program integrated into the FE model for analysing C_a. S1MBA accelerates the back analysis process, enabling designers to examine the range of parameters that best fit data from multiple locations. The study supports the upcoming Brisbane Airport upgrades, enabling optimised and resilient designs for the future, while minimising risk.

KEYWORDS: Parametric study, back analysis, compressible soil, Artificial Intelligence, Genetic Algorithm.

1 INTRODUCTION

Brisbane Airport (BNE) in Australia is built on Holocene-aged alluvium overlying older Pleistocene alluvium, residual soil and rocks of the Petrie Formation. The Holocene layer is further divided into two distinct stratigraphic units: Upper Holocene and Lower Holocene. The Upper Holocene alluvia consist of interlayered clay, silt, and sand, sometimes with peaty inclusions. They are present at the base of sand fill (in aeronautical areas). The presence of sand layers within layers of Upper Holocene Clay (UHC) mean that they settle relatively rapidly compared to the underlying Lower Holocene Clay (LHC), which was laid down in deeper water and tends to be silty clays with minimal persistent layers of sand. The UHC also generally exhibits lower compressibility than the LHC.

These Holocene layers can vary in thickness from 10 to 15 m, with a virgin undrained shear strength ranging from 5 to 25 kPa. They are highly compressible relative to older Pleistocene-aged materials (Indraratna et al. 2011). These uncertainties and spatial variabilities in the compressible soil parameters (and thicknesses) may potentially lead to terminal and runway performance issues, including runway cracking and differential settlement, which may compromise operational safety. A design approach for addressing these uncertainties is through probabilistic assessment (Biram, 2019) or Bayesian back analysis with monitoring using settlement plates or InSAR (Interferometric Synthetic Aperture Radar) to manage both differential and total runway settlement during operation.

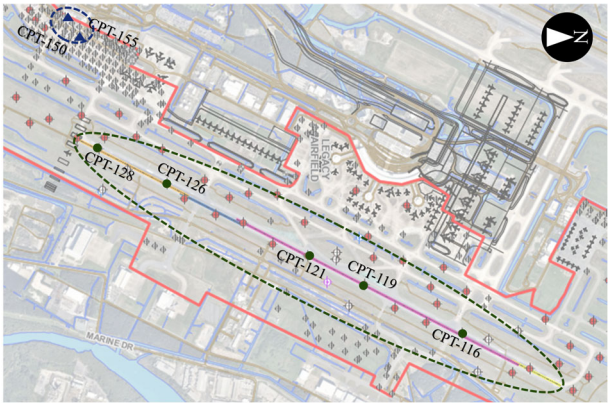

Figure 1. Plan view of Brisbane Airport with CPT locations. The Legacy Airfield runway (LAR) is circled in green, and the historic settlement plates adjoining some location at the International Terminal Brisbane (ITB) is shown in blue (triangle symbol).

The reclamation for the Legacy Airfield runway (LAR) site began in the mid-1980s when sand fill, dredged from Moreton Bay, was placed across the proposed 01R/19L runway, along with its associated taxiways and terminal area (now the Domestic Terminal). The surcharging technique was employed to enhance the ground conditions and mitigate long-term settlements, particularly for primary settlement. The airfield opened in March 1988, and settlement monitoring along the runway centreline has been ongoing since 1991.

Following the opening of the runway and Brisbane Domestic Terminal in 1988, the International Terminal Brisbane (ITB) officially opened in 1995, with construction commencing in early 1993. ITB was historically filled in the early 1990s with dredged sand. The records indicate that a sand embankment approximately 4 m high was placed for about 1 to 2 years within the ITB area. Some historic settlement plate monitoring data are available, and their locations are shown in Figure 1. ITB is approximately 700 m away from the LAR.

Brisbane Airport Corporation (BAC) has upcoming infrastructure projects to prepare for the 2032 Olympics and beyond, including new terminals, taxiways, road upgrades, and land developments (expansions), which will require several ground improvement techniques and efficient geotechnical design. The application of Finite Element Method (FEM) is one of the essential tools for ground improvement designs in BAC's projects, as FEM captures the interaction between soil (with compressible and hardening behaviour, creep), structures (such as piles, Controlled Modulus Columns, and Load Transfer Platforms), and fluid flow (including wick drains and vacuum preloading technique). Understanding the creep parameter, especially for Hypothesis B with S1MBA (Settlement 1-Dimensional Monitoring Back Analysis), is crucial to ensuring the long-term performance and durability of these large-scale constructions.

2 SETTLEMENT IN COMPRESSIBLE SOIL

2.1 *Elastic, Plastic and Viscoplastic*

Elastic settlement in soil refers to the deformation of soil that occurs immediately when it is subjected to a load. It happens instantly after the load is applied, reflecting the soil's immediate response to the stress due to the soil's elasticity (Young's Modulus *'E'* and Poisson's ratio *'v'*). In an FE model, the implication of plasticity can be considered by using an elasto-plastic constitutive model such as the popular Hardening Soil (HS) and Mohr-Coulomb (MC) constitutive model. It is worth

noting that this is mainly considered in the surrounding ('drainage') layers, while the Soft Soil Creep (SSC) model is used for the compressible soils in this study.

In the SSC model, an explicit *E'* is not required because the compressibility behaviour is governed directly by empirical indices: the Compression index 'C_c' and Swelling index 'C_s', which capture the non-linear, stress-dependent stiffness and dominant plastic volumetric strain of soft clays with MC parameters (effective cohesion *c'* and effective frictional angle φ') and pre-consolidation pressure σ'_p, which can be considered in the numerical model using the Over-Consolidation Ratio (OCR) or Pre-overburden Pressure (POP). In addition, these indices can be normalised into the Compression Ratio ($CR = C_c/(1+e_0)$) and Recompression Ratio ($RR = C_s/(1+e_0)$), where e_0 is the initial void ratio. The results are presented in terms of ratios rather than indices in this paper to allow comparison with the published literature.

2.2 *Permeability and Excess Pore Pressure*

Either a surficial load is applied (i.e. fill placed, or footing loads), or the water table is lowered, and the subsurface profile experiences additional stresses beyond the existing overburden stresses. The pore water pressures initially resist these additional stresses. However, these excess pore water pressures dissipate, and the load is gradually transferred to the soil skeleton, increasing the soil's effective stress to match the dissipated excess pore water pressure (Ameratunga, 2021).

In this FE model in Plaxis2D, the *Staged Construction* loading type is used, considering the actual monitoring timeframe, rather than defining the numerical model based on the *degree of consolidation* or *minimum excess pore pressure* over 40 years of monitoring. Since the purpose of the study is to focus on back analysis with the real monitoring data and Hypothesis B, the *Stage Construction* Plaxis2D modelling method is more appropriate.

Additionally, unlike traditional empirical approaches, excess pore pressure in Plaxis2D is numerically generated using Biot's theory of poroelasticity in the *Undrained effective stress analysis*. A critical characteristic of the FEM is that the rate of excess pore pressure depends on the bulk modulus and compressibility of both the pore water and the soil skeleton, as well as the volumetric strain rate. In the SSC model, excess pore pressure can continue to develop in response to ongoing volumetric strains, which may also represent time-dependent creep behaviour.

In Plaxis2D, vertical permeability 'k_v' is used as an input rather than the coefficient of consolidation 'C_v'. A common method that uses a fundamental theoretical relationship is presented in Ameratunga (2021, pp. 39, pp. 81) in Equation (1):

$$k_v = xk_h = C_v.\gamma_w.m_v = C_v.\gamma_w.\frac{0.434.CR}{\sigma'_{avg}} \qquad (1)$$

where γ_w is the unit weight of water, m_v is the coefficient of volume compressibility, and σ'_{avg} is the average vertical normal stress during consolidation. Bell (2000) stated that normally consolidated alluvial clays have m_v value range from 0.3 to 1.5 MPa^{-1}.

2.3 *Secondary Compression (Creep) – Hypothesis A vs B*

In the prediction of creep, the contribution of secondary compression is considered under two hypotheses. Hypothesis A (H-A) and B (H-B). The left diagram in Figure 2 shows that an additional stress increment shifts the soil state from its initial effective stress. H-A assumes that secondary compression begins only after primary consolidation is complete, resulting in an increase in vertical strain along the instant compression line, followed by creep settlement once the full effective stress is reached. In contrast, H-B captures that creep occurs concurrently with primary consolidation, producing a more continuous strain path during the stress increment.

Figure 2 (right) highlights that H-A predicts a distinct transition from primary to secondary settlement, while H-B gives a smooth, continuous strain curve where time-dependent deformation starts from the moment of loading. This distinct transition becomes more pronounced with increasing compressible soil thickness.

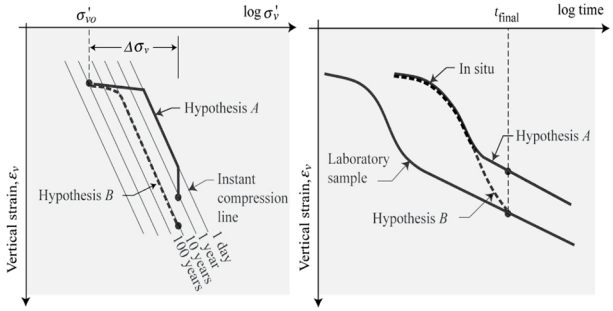

Figure 2. H-A versus H-B (Ladd et al. 1977), Vertical Strain against (Left): Vertical Stress, (Right): Time in log scale.

Regardless of the assumption, the fundamental secondary compression remains the same, relating creep settlement to the logarithmic ratio of time intervals as shown in Equation (2):

$$S_c = \frac{C_a}{1+e_0} H \log\frac{t_f}{t_{PEnd}} \qquad (2)$$

where S_c is the creep settlement, H is the thickness of the compressible soil, t_f is the design life, and t_{PEnd} is the end of primary consolidation. The relationship between $C_{a,A}$ (the C_a for H-A) and $C_{a,B}$ (the C_a for H-B) for back analysis purposes is presented in the Equation (3). It assumes that both creep components of H-A and H-B are the same since S_c is monitored:

$$\frac{C_{a,A}}{C_{a,B}} = \frac{\log t_f - \log t_{PEnd,B}}{\log t_f - \log t_{PEnd,A}} \qquad (3)$$

where subscript $_A$ is used for the H-A and $_B$ for the H-B. Theoretically, $t_{Pend,\,B}$ is within days compared to $t_{Pend,\,A}$ ($t_{Pend,\,A} >> t_{Pend,\,B}$). Figure 3 presents the potential scenarios of the Equation (3) where t_f is the current monitoring date and $t_{PEnd,\,A}$ is between 0.5 to 3 yrs are plotted along the x-axis. Then the $t_{PEnd,\,B}$ assuming creep starts at Day 1. The potential difference between the creep parameters of H-A and H-B can be read from the y-axis. When settlement back-analysis is performed using field measurements, $C_{a,\,A}$ has a higher value than $C_{a,\,B}$ (assuming all other parameters are consistent). The careful consideration of these alternative assumptions is crucial in the design and implementation of ground improvement strategies, particularly for methods intended to accelerate the primary consolidation process within a short timeframe.

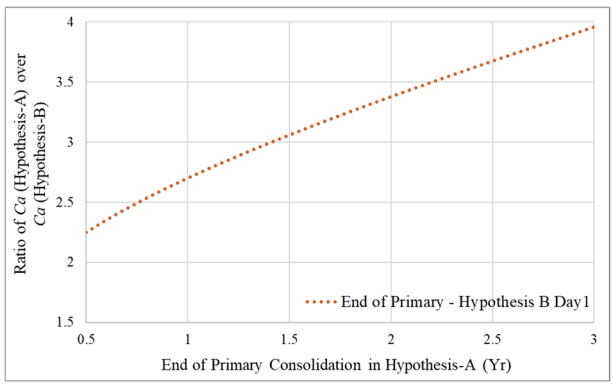

Figure 3. Ratio of $C_{a,\,A}$ and $C_{a,\,B}$ for back analysis varying by year at the end of primary in H-A.

3 GEOTECHNICAL AND MONITORING DATA

3.1 *Legacy Airfield's Back Calculated Ground Profile*

Historical geotechnical data available for the Legacy Airfield runway (LAR) from the 1980s are limited. A detailed geotechnical investigation was undertaken along the 01R/19L runway in early 2023 to minimise this uncertainty and inform any future development or upgrades across the area. Cone Penetration Tests (CPTs) were completed in 2023 at the LAR, which provided current stratigraphy at discrete locations along the runway. Their derived stratigraphy was then adjusted to represent 1982 conditions by accounting for the settlement caused by the sand embankment, supported by original site clearing plans and base level comparisons. The CPT numbers are 116, 119, 121, 126 and 128 (Refer to Figure 1), and Table 1 provides back-calculated ground profiles adjusted from the settlement readings.

3.2 *Historical Ground Profile for ITB*

ITB was constructed several years after the Legacy Airfield's opening (in the early 1990s), and its geotechnical data contain valuable information. It includes a detailed geological ground profile (thickness of UHC, LHC and Drainage layers) and laboratory results such as *CR*, $C_{\alpha\varepsilon}$, and C_v. From these historical data, CPT 150 and 155 were used (see Figure 1). Figure 4 shows the historical laboratory data with the sample depths. The green-shaded region indicates UHC, whereas the rest are potentially LHC, due to reduced permeability and increased compressibility in the test results.

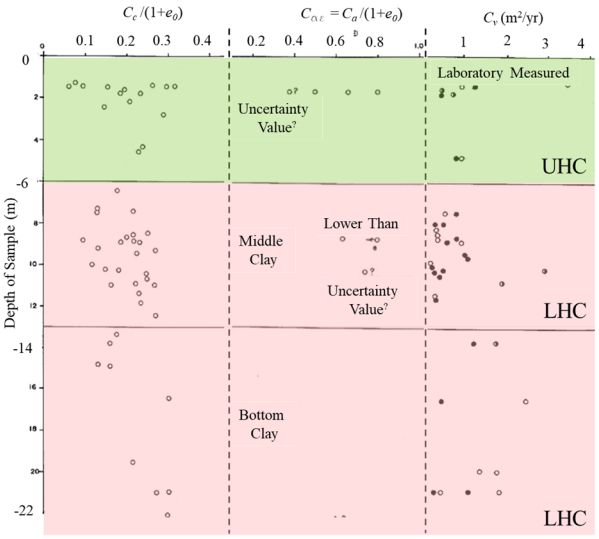

Figure 4. Historical laboratory data from the early 1990s. Table 1 provides historical ground profiles.

Table 1. Surface RL (m) interpreted from CPT Data. Note [1]: D – Clayey Sand or Fill (Sand) as a Drainage layer, [a]: ITB location, and [b]: Runway.

CPT	150[a]	155[a]	116[b]	119[b]	121[b]	126[b]	128[b]
D[1]	2.6	2.5	-	-	-	-	-
UHC	1.8	2.0	2.0	1.8	1.8	2.1	1.7
D[1]	-2.4	-1.5	-1.4	-1.2	-1.3	0.9	-0.5
UHC	-	-	-3.1	-5.5	-4.0	-	-
LHC	-4.4	-4.3	-5.3	-	-	-	-4.7
D[1]	-	-	-9.2	-11.8	-7.4	-	-12.5
LHC	-	-	-9.5	-15.6	-14.9	-4.1	-15.2
D[1]	-11.6	-11.0	-16.4	-21.7	-23.7	-14.0	-19.6

3.3 *Loading History and Monitoring Data*

3.3.1 *Legacy Airfield Data for Back-Analysis*

Historical construction records, surveys, satellite imagery, and aerial photos were carefully filtered and analysed to establish baseline conditions in 1982, including load history and embankment details. The details of the sequencing are presented in Table 2. The monitoring data have been recorded from 1991 to the present time. The primary challenge of this study is the lack of monitoring data for the surcharging period during construction from 1982 to 1985. Five data points are used in S1MBA; they are the settlement readings from the runway opening in 1985, and from 1991, 2004, 2014, and the present, as shown in Figure 5.

Table 2. Modelling Sequence for Legacy Airfield. Note [1]: Used the elevation reference, and [2]: Use the monitoring data from 1991.

Stage	Remarks
November 1982: Start of Construction	Sand was dredged and placed to build a surcharge up to approximately RL 6.5m.
January 1985: Surcharge Removal	After 2 years, the surcharge was partially removed to RL 5.1m[1].
May 1987: Application of Pavement[1,2]	The pavement (i.e., service load) was applied.
February 2004: Pavement Top-up[2]	A top-up between 20mm and 70mm was applied.
April 2014: Pavement Top-up[2]	Further topping up was applied between 10mm and 20mm.

In Figure 5, the monitoring settlement data are plotted against time on a log scale. The thickness of the UHC and LHC layers is presented in the Table 3 together with the monitored creep rate over 30 to 40 years. However, the settlement in 1991 is assumed to be the elevation difference between the design RL and the recorded elevation in 1991.

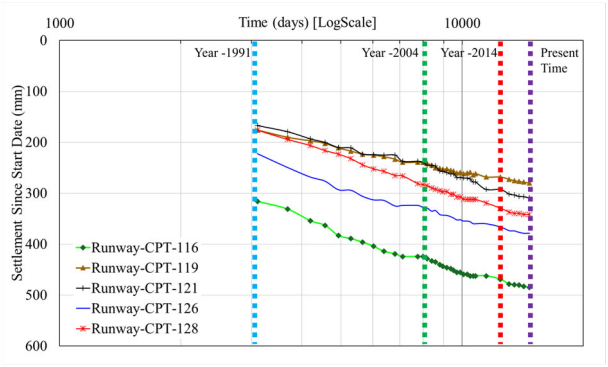

Figure 5. Legacy Airfield Monitoring Data from 1991 to the current time. Start Day 0 means before ground improvement.

$$C_{\alpha\epsilon} = \frac{C_a}{1+e_0} = \frac{S_c}{H \log\frac{t_f}{t_{PEnd}}} = \frac{S_{Monitored\ Data}}{H \log\frac{t_f}{t_{PEnd,A}}} \quad (4)$$

Table 3. Legacy Airfield CPT with its compressible soil thickness, and back-calculated $C_{\alpha\varepsilon,A}$ using the Equation (4) with monitoring. Note [1]: Assumed that *CR* for LHC is 0.24 (Refer to Figure 11).

CPT	Thickness (m)		Monitoring Settlement (mm)	$C_{\alpha\varepsilon,A}$ (%)	$C_{\alpha\varepsilon,A}/CR^1$
	UHC	LHC			LHC
116	5.6	10.9	169.1	1.6	-
119	9.3	6.1	103.5	1.0	-
121	6.5	8.8	141.8	1.4	-
126	1.2	9.9	156.6	1.9	0.08
128	2.2	12.2	165.8	1.7	0.07

Equation (2) is rearranged into Equation (4) and replaced with monitoring data to calculate a performance based $C_{\alpha\varepsilon,A}$, assuming both UHC and LHC have the same creep properties. The results highlighted that the thicker the LHC layer, the higher the amount of creep over time, whereas the creep amount decreases with increasing thickness in UHC. This outcome supports the initial design assumption that UHC exhibits lower compressibility (both primary and secondary) than the LHC.

3.3.2 *ITB Data for Primary Consolidation*

Since the primary aim of this study is to find the representative $C_{a,B}$ of the project site, it is not a correct approach to ignore the primary settlement period. Therefore, alternative data for the International Terminal Building (ITB) was reviewed to correlate primary consolidation parameters. However, ITB only has the primary loading period from the construction stage (i.e. no ongoing monitoring is available). The settlement analysis uses the historical settlement plate monitoring data (see Figure 6) during the 1992 site surcharging, and inferred stratigraphy from nearby CPT 150 and 155 is used (see Figure 1). These data were incorporated into the sequence and tabulated into the data format. It is to highlight that only the data from the red dots are used for S1MBA, where the loading history is also shown in Figure 6.

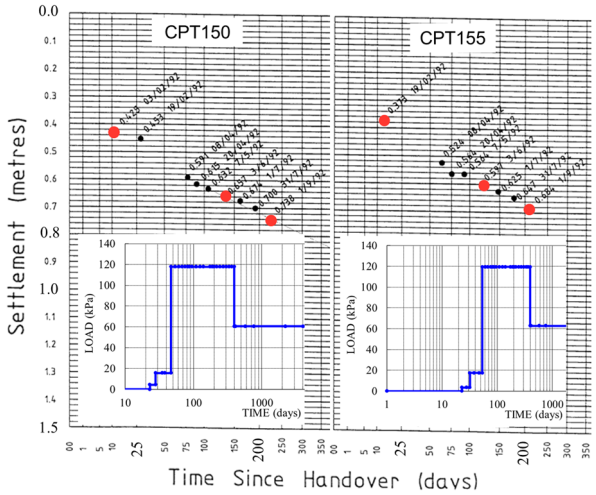

Figure 6. Historical Settlement Plate Data at ITB in 1992 and assumed load history for ITB (CPT 150 and CPT 155).

The floor slab in ITB is designed in the 1990s to settle separately from the pile cap, on which the piles bear below the Pleistocene alluvia. In 2023, it was recorded that the floor slab at ITB has settled between 150 to 175 mm since 1995, which is likely due to creep. This information is considered in S1MBA.

3.4 *Groundwater*

Groundwater across the Legacy Airfield is variable and is expected to have been near the surface prior to the development in the 1980s. At the ITB, groundwater was recorded at an approximate depth of 2.2 m below natural surface level in October 1991. This measurement was taken before the surcharge fill was applied. Post development, groundwater levels across the airport are expected to be within the sand fill. In a subsequent investigation conducted in 2005 (at the ITB), groundwater was noted at an approximate depth of 2.0 m below the ground surface (which was approximately 1.5 m higher than natural surface level). Groundwater data across the Legacy Airfield (from insitu VWPs and from CPT data) indicate groundwater levels between 1.0 m and 2.0 m below the surface. Groundwater levels are expected to fluctuate in response to rainfall and tidal changes; however, this is not expected to significantly impact the settlement unless prolonged changes are expected.

3.5 *Existing Data, Challenges and Innovation*

Legacy Airfield data only provides information on the secondary compression parameters of the underlying clays as primary settlement is expected to have been completed prior to monitoring in 1991. Whereas the ITB data has settlement records during surcharging (which inform primary consolidation parameters).

Since $C_{a,B}$ starts from the beginning of the ground improvement stage, neither piece of information is directly fit for back analysis purposes. However, a significant assumption made in this paper is that these locations are in similar proximity and have the same geological lithology and similar primary consolidation parameters. Furthermore, a database of monitoring data and laboratory testing is available across the Brisbane Airport site from developments since the 1980s (Biram, 2019)

Suppose the objective is to achieve the design parameters that fit the monitoring data, the standard approach is to utilise the geotechnical engineer's previous design experience and conduct several trials and errors through numerous modelling simulations. It can be time-consuming to solve, and the potential for better design options may be limited to the engineer's previous design experience. In this paper, these challenges are overcome by using S1MBA.

4 GENETIC ALGORITHM AND S1MBA

Genetic Algorithm (GA) uses an analogy to Darwin's theory of evolution, aiming to improve a set of parameters (C_c, C_s, and C_a, as well as OCR and k_v) to obtain even better sets according to a particular goal. GA is a popular optimisation technique widely used, particularly in engineering due to its relative simplicity and minimal requirements for problem formulation (Tun, 2018). It needs only an objective function in the Equation (5) with a set of constraints. S1MBA is the WSP's in-house programme, which integrates GA and Plaxis2D (see Figure 7). All the annotations related to the GA algorithm will be defined with the $_{GA}$ subscript.

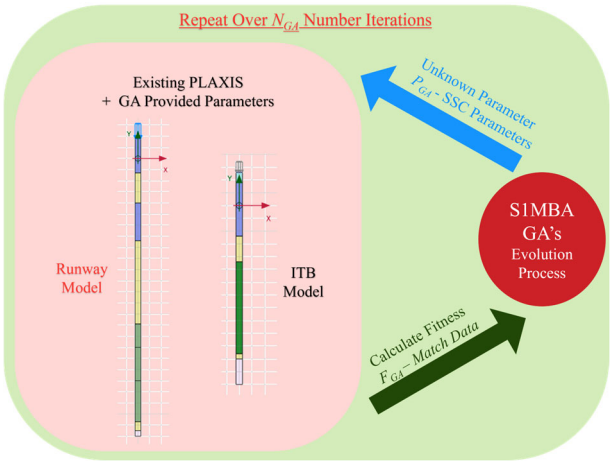

Figure 7. Implementation Flowchart for S1MBA and Plaxis2D.

4.1 *Objectives and Fitness Function, F_{GA}*

In simple mathematical terms, back analysis is fitting two curves plotted on two axes (Figure 8). These curves are plotted between settlements (y-axis) against time (x-axis). It is challenging for engineers or GA to define which parameters are calibrated well, or in other words, what calibration gives the best Fitness value (F_{GA}).

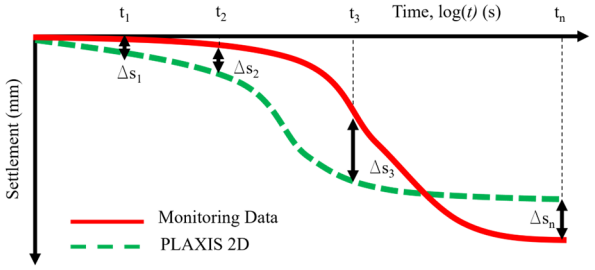

Figure 8. Visual mathematical illustration of the objective function.

This paper proposes that the fitness value F_{GA} can be calculated by the Fitness function (F_{PGA}) shown in the Equation (5). This equation can be used independently assess the accuracy of the back-analysis results.

$$F_{PGA} = \frac{\sum_0^{n=Points} |s_{\ Settlement\ Plate} - s_{PLAXIS2D}|}{n = number\ of\ data\ points} \qquad (5)$$

First, 'Δs' calculates the difference between Settlement '$s_{\ Settlement\ Plate}$' from settlement plate data and Plaxis2D '$s_{PLAXIS2D}$' results for each date ($t_1, t_2, t_3, \ldots, t_n$). Then, divide the absolute value of $|\Delta s|$ by the total number of recorded dates (data). This will be the Fitness function 'F_{PGA}', and GA will minimise the F_{PGA}, closing the gap between the $s_{settlement\ plate}$ and $s_{PLAXIS2D}$.

4.2 *Mutation and Constraints*

Theoretically, one set of parameters may match the monitoring data (i.e. result in a low F_{PGA} value), but the actual individual parameter values may not be consistent with common relationships in practice. For example, the program may produce a set of parameters for an individual layer with low C_a value and high C_c, which does not comply with typical ratios, such as those published by Mesri et al. (1994). There may be many other parameter combinations that fit the same monitoring data by simply adjusting the permeability and *OCR*.

Without proper engineering judgement, the relative compressibility or permeability of the UHC and LHC may also conflict to our understanding of soil behaviour (i.e. UHC has a lower compressibility than LHC). To achieve realistic results, it is important to provide the right amount of mutation and define project-specific constraints.

To capture a wide variety of parameter sets in multimodal optimisation problems, a higher mutation rate is recommended. The algorithm effectively explores less-visited regions of the search space, uncovering alternative optima that might otherwise remain undetected by introducing randomness (Tun, 2018).

5 PLAXIS2D – 1D NUMERICAL MODEL

A one-dimensional consolidation modelling approach is implemented in Plaxis2D. The model geometry is designed to balance computational efficiency with the need for accurate representation of the physical process. In the Plaxis2D 1D-validation, the soil column has a height of 15 to 20 m and a width of 0.5 m, which effectively eliminates lateral flow effects while providing a sufficient vertical domain for consolidation behaviour.

The side boundaries of UHC and LHC are modelled as impermeable, ensuring vertical drainage through the top and bottom only, allowing pore water to dissipate freely. This compact model size enables the accurate replication of the theoretical solution with minimal computational demand. The *Undrained-A* from the SSC model is used with the MC calibrated parameters (c' and φ') that represent the virgin undrained shear strength (S_u).

Table 4. Geotechnical Design Parameters. Note [1]: D – Clayey Sand or Fill (Sand) as a Drainage layer, and [2]: SSC Model.

	γ (kPa)	E' (MPa)	v' / v'$_{ur}$	c' (kPa)	φ' (deg)	e_0	OCR
D[1]	19.0	20	0.20	5	32	0.5	-
UHC	17.4	n/a[2]	0.15	2	28	1.5	1.2-1.1
D[1]	19.0	15	0.30	1	30	0.5	-
LHC	16.2	n/a[2]	0.15	2	26	1.7	1.1-1.0
Rock[1]	24.0	1000	0.20	20	36	0.5	-

6 DESIGN METHODOLOGY

The design flow for this study begins with developing a FE model using the virgin ground condition as the baseline. The model is then staged to replicate the load history derived from long-term settlement monitoring data (refer to Section 3.3). SSC design parameters, along with other critical soil parameters, were back-analysed, including *Cc*, *Cs*, k_v, C_a, and OCR (Refer to Section 2).

Initial parameter ranges are assigned for both UHC and LHC, with practical constraints such as enforcing higher permeability for UHC relative to LHC. This is critical to achieving a realistic result as design parameters must be constrained by understanding the soil's true behaviour. These constraints are based on literature, historical laboratory and field data and back-analysis of previous surcharge embankments across the airport (refer to Section 2 and 3).

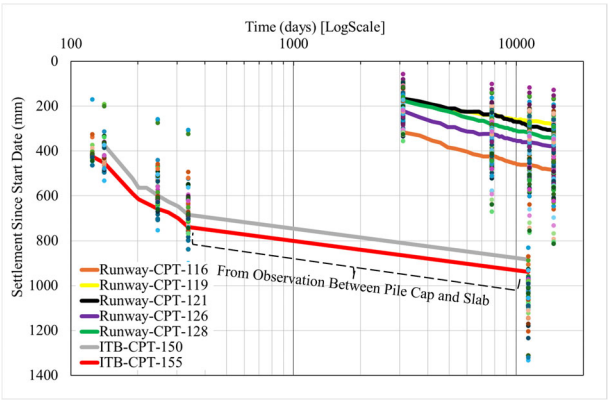

Figure 9. GA Evolution 1: Generated parameter sets from the provided design parameter range.

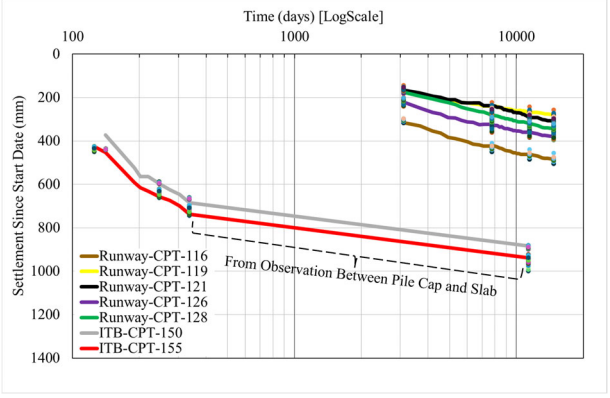

Figure 10. GA Evolution Final: Optimised parameter sets matching the monitoring data.

S1MBA's GA is employed to search for optimal parameter sets iteratively. Its framework specifies the number of simulations,

mutation rates, and other parameters. The initial GA runs use parameter sets that do not match the monitoring data, as illustrated in Figure 9, where solid lines represent monitoring data and dots denote Plaxis2D results for initial GA predictions. Through successive generations, these Plaxis2D results track towards the observed settlement behaviour (see Figure 10). Once the GA evolution converges, all output data is stored for further engineering review.

7 RESULTS AND DISCUSSION

In total, more than 3000 Plaxis2D simulations with different parameter sets were run. Among them, 823 parameter sets result in a fitness value within ± 25 mm (based on monitoring accuracy). These parameter sets are then visualised in histograms to illustrate the likely distribution and range of filtered soil properties that match the monitored settlements, which will inform future design (see Figure 11 to Figure 13).

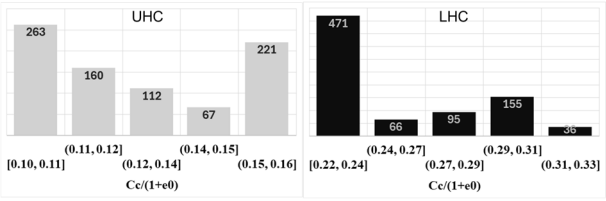

Figure 11. Filtered GA results for $CR = C_c/(1+e_0)$.

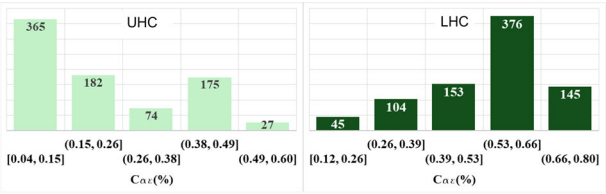

Figure 12. Filtered GA results for $C_{\alpha\varepsilon}$(%).

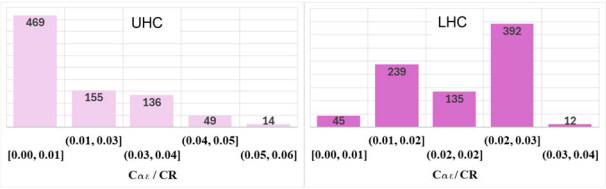

Figure 13. Filtered GA results for $C_{\alpha\varepsilon}/CR$.

A comparison of the derived *CR* ranges shows good alignment with the parameter ranges from Biram (2019), while within the range shown in Figure 4. Biram defines a range from 0.10 to 0.25 for UHC and 0.15 to 0.35 for LHC. GA-filtered results in Figure 11 indicate that most simulations converge within the ranges of 0.11 - 0.12 (with 263 simulations) and 0.15 - 0.16 (with 221 simulations) for UHC. In the LHC, most acceptable solutions fall between 0.22 and 0.24, based on 471 simulations.

Biram (Hypothesis A) assumes a range for $C_{\alpha\varepsilon}$ of 0.3 to 1.0% for UHC and 0.8 to 1.2% for LHC. GA-filtered results in Figure 12 (Hypothesis B) indicate that UHC $C_{\alpha\varepsilon}$ values mainly fall below 0.15%, while LHC clusters between 0.26% to 0.66%, with a peak around 0.53% to 0.66%.

The monitoring data simplistically back calculated in Table 3 shows values between 1.0% and 1.9%, which are higher than those recommended by Biram for Hypothesis A. The back-analysed (with FEM) Hypothesis B creep parameters are about 35% to 50% of Hypothesis A '$C_{\alpha\varepsilon}$'. These results show a similar outcome to the assumptions stated in Figure 3.

Mesri et al. (1994) provide recommendations for the ratio of $C_{\alpha\varepsilon}/CR$ for inorganic clays and silts of 0.04 ± 0.01. The results from this study indicate for Hypothesis B, a ratio (for the majority of 'fitted' simulations) of about 0.02 ± 0.01 for both UHC and LHC. Initial review of Hypothesis A parameters (comparing Table 3 to the most likely values of *CR* by Biram and Figure 11) indicate a much higher ratio (up to 0.08).

8 CONCLUSIONS

This study has adopted long-term real world monitoring data to estimate secondary compression parameters for the Holocene clays at the Brisbane Airport. The results highlight that it is important to adjust these parameters, depending on the model assumptions (i.e. adopting either Hypothesis A or Hypothesis B).

The modelling confirms that Hypothesis A creep parameters are typically about two to three times higher than those calculated under Hypothesis B. Directly applying these higher values in finite element models with Soft Soil Creep can therefore lead to overly conservative settlement predictions and potentially unnecessary design costs.

Furthermore, when modelling secondary compression, adopting the Hypothesis A theory, higher creep parameters than those adopted by Biram (from laboratory results) are recommended for clays at the Brisbane Airport. To improve reliability, it is essential not to depend on a single dataset. Instead, combining multiple sources of data and adopting a probabilistic approach provides a more realistic representation of possible soil behaviour.

The integration of the S1MBA tool with FEM software (Plaxis 2D) demonstrates a promising framework for more efficient geotechnical design in compressible soils. Using larger sample sizes with multiple GA iterations and clearly defined user constraints helps ensure robust, realistic outputs that support better engineering decisions.

9 ACKNOWLEDGEMENTS

The author would like to express deepest appreciation to Dr. Scott Fidler for his mentoring on the projects. The author acknowledges Dr. Ardie Purwodihardjo, Krystle-Rae Biram, and Yohanne Faivre for their support of the International Brisbane Terminal Study. The support from the Brisbane Airport Corporation and WSP is gratefully acknowledged.

10 REFERENCES

Ameratunga, J., Sivakugan, N., and Das, B. 2021. *Soft clay engineering and ground improvement*. London: Taylor & Francis

Bell, F.G. 2000. *Engineering Properties of Soils and Rocks*. 4th ed, Oxford: Blackwell Science.

Biram, K., 2019. Surcharge design using a probabilistic framework. *Proceedings of the 13th Australia New Zealand Conference on Geomechanics*, Perth, Western Australia, Australia, 1-3 April, Australian Geomechanics Society, 571-575.

Indraratna, B., Ameratunga, J., Boyle, P. & Rujikiatkamjorn, C. 2011. Performance and prediction of vacuum combined surcharge consolidation at Port of Brisbane. *Journal of Geotechnical and Geoenvironmental Engineering* 137(11), 989–1131.

Ladd, C.C., Foott, R., Ishihara, K., Schlosser, F. and Poulos, H.G. 1977. Stress-deformation and strength characteristics. *Proceedings of the 9th International Conference on Soil Mechanics and Foundation Engineering*, Tokyo, 2, 421–494.

Mesri, G. and Godlewski, P.M., 1977. Time and stress compressibility interrelationship, *Journal of Geotechnical Engineering Division*, 103(GT5), 417–430.

Mesri, G., Lo, D.O.K. and Feng, T.W., 1994. Settlement of embankments on soft clays. In: ASCE, *Vertical and Horizontal Deformations of Foundations and Embankments: Settlement '94, Geotechnical Special Publication No. 40*. College Station, Texas, 16–18 June, New York: ASCE, Vol. 1, pp.8–56.

Tun, Y., Llano-Serna, M.A., Pedroso, D.M. and Scheuermann, A. 2018. Multimodal reliability analysis of 3D slopes with a genetic algorithm. *Acta Geotechnica*, 14(1), 1-17.